Bioinspiration & Biomimetics

RECEIVED
5 August 2015

REVISED
17 October 2015

ACCEPTED FOR PUBLICATION
22 October 2015

PUBLISHED
18 November 2015

PAPER

Hydrodynamic function of biomimetic shark skin: effect of denticle pattern and spacing

Li Wen[1,2,4], **James C Weaver**[3], **Patrick J M Thornycroft**[2] **and George V Lauder**[2,4]

[1] School of Mechanical Engineering and Automation, Beihang University, Beijing, 100191, People's Republic of China
[2] The Museum of Comparative Zoology, 26 Oxford St., Harvard University, Cambridge, MA 02138 USA
[3] Wyss Institute for Biologically Inspired Engineering, Harvard University, Cambridge, MA 02138, USA
[4] Author to whom any correspondence should be addressed

E-mail: liwen@buaa.edu.cn **and** glauder@oeb.harvard.edu

Keywords: hydrodynamics, shark skin, robot, denticle, 3D printing

Abstract

The structure of shark skin has been the subject of numerous studies and recently biomimetic shark skin has been fabricated with rigid denticles (scales) on a flexible substrate. This artificial skin can bend and generate thrust when attached to a mechanical controller. The ability to control the manufacture of biomimetic shark skin facilitates manipulation of surface parameters and understanding the effects of changing denticle patterns on locomotion. In this paper we investigate the effect of changing the spacing and arrangement of denticles on the surface of biomimetic shark skin on both static and dynamic locomotor performance. We designed 3D-printed flexible membranes with different denticle patterns and spacings: (1) staggered-overlapped, (2) linear-overlapped, and (3) linear-non-overlapped, and compared these to a 3D-printed smooth-surfaced control. These 3D printed shark skin models were then tested in a flow tank with a mechanical flapping device that allowed us to either hold the models in a stationary position or move them dynamically. We swam the membranes at a frequency of 1 Hz with different heave amplitudes (from ± 1 cm to ± 3 cm) while measuring forces, torques, self-propelled swimming speed, and cost of transport (COT). Static tests revealed drag reduction of denticle patterns compared to a smooth control at low speeds, but increased drag at speeds above 25 cm s^{-1}. However, during dynamic (swimming) tests, the staggered-overlapped pattern produced the fastest swimming speeds with no significant increase in the COT at lower heave values. For instance, at a heave frequency of 1 Hz and amplitude of ± 1 cm, swimming speed of the staggered-overlapped pattern increased by 25.2% over the smooth control. At higher heave amplitudes, significantly faster self-propelled swimming speeds were achieved by the staggered-overlapped pattern, but with higher COT. Only the staggered-overlapped pattern provides a significant swimming performance advantage over the smooth control and the other two denticle patterns. Quantitative hydrodynamic comparisons among skin models where control over manufacture allows alteration of design parameters provides a useful experimental tool for future work on the considerable natural diversity of shark skin denticles both among species and on different body locations.

1. Introduction

Sharks are well-known for their rough skin which is composed of rigid bony denticles (or scales) embedded into the epidermis and dermis (Applegate 1967, Reif and Dinkelacker 1982, Reif 1985, Kemp 1999, Meyer and Seegers 2012, Motta *et al* 2012, Díez *et al* 2015). These denticles are composed of tooth-like layers of enameloid and dentine with a central pulp cavity, and have an expanded base that anchors individual denticles into the skin. Although there is a great variety of denticle shapes and spacing patterns in different shark species, and considerable variation around the body (Reif 1985, Wen *et al* 2014, Díez *et al* 2015), at the mid-body area and on many of the fin surfaces of pelagic sharks the denticles have a plate-like upper section

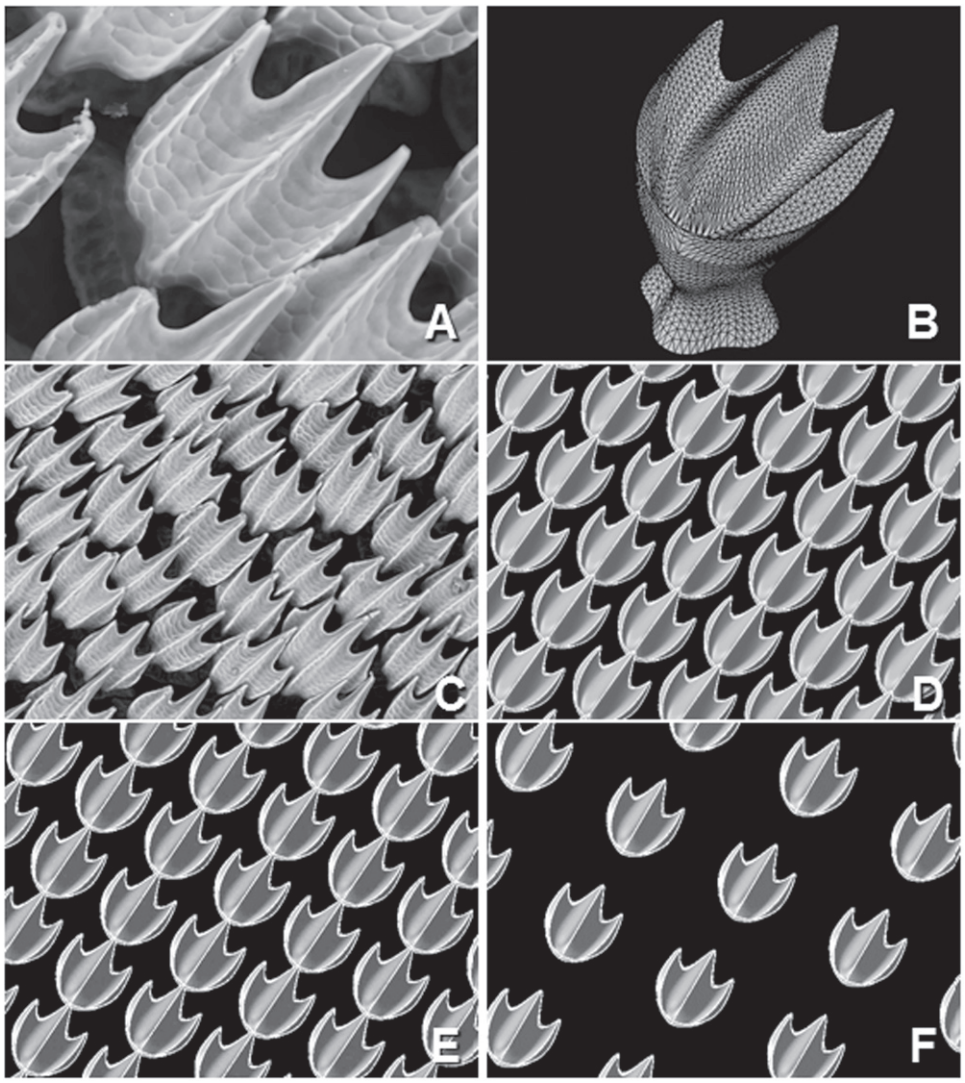

Figure 1. Zoomed-in and wide-view environmental scanning electron microscope (ESEM) images of denticles taken from skin pieces extracted at the positions of the anal fin (a) and (c) of the bonnethead shark (*Sphyrna tiburo*). Denticle length in (a) and (c) is approximately 130 μm. Three-dimensional reconstructed micro-CT model of a single denticle (showing the meshed surface) is shown from a 45° angled view (b). Note the expanded base which is embedded into the flexible membrane during 3D printing. This model represents a modified version of denticles that contains shape elements from both bonnethead and mako sharks and exaggerated elements to allow more accurate 3D printing (see materials and methods). SolidWorks model of the staggered-overlapped skin denticle array (d). The linearly-overlapped and non-overlapped arrayed shark skin models are shown in (e) and (f).

bearing ridges which narrows to a thin neck that enters the skin, expanding into a base plate (figures 1(a)–(c)). The upper portions of denticles overlap each other, and each denticle in this region thus has an overhanging section which overlaps the next downstream denticle.

The intricate structure of individual denticles and their complex patterning on the skin surface has stimulated a number of engineering studies on the hydrodynamic effects of simplified model shark denticles. This work has focused on measuring drag during static tests to determine if a denticle-like roughened surface could reduce drag during locomotion by analogy to riblet structures, which have been extensively studied for engineering applications (e.g., Anderson *et al* 1997, Bechert *et al* 1997, Bhushan 2011, Büttner and Schulz 2011, Dean and Bhushan 2010, Zhao *et al* 2012). And recently Díez *et al* (2015) completed a computational fluid dynamic analysis of the effect skin surface roughness on a model shark body in relation to lift and drag forces.

But analyses of highly simplified riblet-like models of shark denticles under static conditions can not replicate the hydrodynamic environment that occurs during undulatory propulsion during which the body, fins, and tail are moving in complex three-dimensional patterns (Webb and Keyes 1982, Wilga and Lauder 2000, 2002, Borazjani and Daghooghi 2013). Such movements induce complex flows over the skin surface (Anderson *et al* 2001) greatly complicating the inference of locomotor performance effects of specific skin features from static tests alone. In order to tease apart the effects of different denticle shapes and patterned arrangements on the skin, we need

experimental control over denticle configurations, and the ability to test these denticle patterns under swimming conditions in which locomotor kinematics and forces can be measured, and derived quantities such as swimming speed and cost of transport (COT) calculated.

We recently developed a method for manufacturing a biomimetic flexible shark skin panel covered with rigid denticles, and studying the dynamics of propulsion in this membrane (Wen *et al* 2014). Wen *et al* (2014) used a mechanical flapping controller, developed to study propulsion under controlled experimental conditions in a variety of flexible materials (e.g., Alben *et al* 2012, Lauder *et al* 2012, Wen and Lauder 2013, Shelton *et al* 2014, Feilich and Lauder 2015), to quantify undulatory kinematics, self-propelled swimming speed, locomotor forces, and the COT of a panel with biomimetic denticles compared to a smooth-surfaced control. This experimental system permits quantitative comparisons among membranes with different surface structures under dynamic swimming conditions that replicate those of freely-swimming sharks (Oeffner and Lauder 2012, Lauder and DiSanto 2015). Wen *et al* (2014) studied the hydrodynamic effect of one surface pattern compared to a smooth control, but did not investigate the effect of changing denticle spacing and overlap with adjacent denticles.

The goal of this study is to use our ability to manufacture biomimetic shark skin to test the comparative swimming performance of three different denticle patterns relative to a smooth control surface. We chose one denticle shape, arrayed this shape in three different patterns, and used multimaterial additive manufacturing to print rigid denticles onto flexible panels which were then assembled into two-layer membranes for testing. We performed both static drag and dynamic swimming tests of locomotor performance with the goal of understanding the functional significance of denticle arrangements in shark skin. Dynamic experiments allowed us to test the hypothesis that surface denticles increase self-propelled swimming speeds, to understand the effects on swimming speed of changing patterning, and to determine how the COT for each pattern changes relative to a smooth control surface.

2. Materials and methods

2.1. Design and fabrication of biomimetic shark skin patterns

Shark skin denticles (or scales) were examined from two species as the basis for making a custom, generic, 3D denticle model in SolidWorks. Environmental scanning electron microscope (ESEM) images of the bonnethead shark (*Sphyrna tiburo*) skin surface were taken from skin pieces extracted at a position near the anal fin, and images of denticles at several body locations were taken from a freshly dead specimen of the Shortfin Mako shark (*Isurus oxyrinchus*, Rafinesque). For example, a top-view ESEM image is shown in figure 1(a) to illustrate details of the three-dimensional structure of bonnethead shark denticles. To assist in generating a quantitative three-dimensional model of a single shark skin denticle, we also extracted a small piece of shark skin (2 mm $\times$ 2 mm) of a male Shortfin Mako shark (*Isurus oxyrinchus*, Rafinesque) and used a microcomputed tomography (μ-CT) scanner (Xradia VersaXRM-500, at Cornell University, Institute of Biotechnology) at a resolution of 1.58 μm in the x, y, and z directions. We picked a single representative skin denticle from this scan and constructed a 3D model which was then covered in a digital mesh using Mimics 3D modeling software (Materialise Inc., Belgium), as shown in figure 1(b). This 3D model assisted in designing a custom 3D SolidWorks model which was used for 3D printing as described below. Further details of the three-dimensional reconstruction of a single denticle are provided in our previous study (Wen *et al* 2014). The reconstructed denticle model represents an abstracted and somewhat generic denticle shape representative of several species, but not specifically modeled on any one species. This model was then duplicated and arrayed in three controlled patterns, described below, on a membrane substrate in SolidWorks (SolidWorks Corp., Waltham, MA, USA).

Denticle distributions on a samples of real shark skin showed variation in the spacing and pattern of the denticles on the surface (e.g., figure 1(c)). We constructed simplified generic versions of arrays of shark denticles using three different patterns and tested these against a smooth control. We term these (1) the staggered-overlapped array (figure 1(d)), (2) the linear-overlapped array (figure 1(e)), and (3) the linear-non-overlapped array (figure 1(f)). Quantitative parameters (S_s and S_l) that govern denticle spacing, the number of denticles and the surface area of the models compared among the different patterns, are listed in table 1 and illustrated in figure 3. S_s indicates the spacing between two adjacent denticles along the streamwise direction, and S_l indicates spacing between the mid-ridges of two adjacent denticles in the lateral direction.

To fabricate a synthetic shark skin membrane, we used the Objet Connex500 3D printer (Stratasys Ltd, Eden Prairie, MN, USA). Two different materials, printed together in one operation, were used for fabricating the model that contained both rigid (for the denticles) and flexible (for the membrane substrate) components. Based on our previous work using manufactured biomimetic shark skin (Wen *et al* 2014), it was critical to embed the rigid denticles into the flexible membrane, and for the manufactured panel to be able bend and generate thrust when moved dynamically using the mechanical controller described below. In addition, a soft, gel-like supporting material was

Table 1. Morphological parameters of the smooth control and synthetic shark skin membranes. S_s and S_l are defined in the caption of figure 3.

Shark skin morphology	Control	Staggered-overlapped	Linear-overlapped	Linear- non-overlapped
S_s (mm)	—	2.05	2.05	3.08
S_l (mm)	—	2.05	2.05	3.25
Number of denticles	0	2352	2160	960
Denticle surface area (mm^2)	0	20 030	18 395	9710
Membrane surface area (mm^2)	10 420	8681	8823	8175
Total surface area (mm^2)	10 420	28 711	27 218	17 886

used to allow fabrication of overhanging denticles by providing a temporary surface to support 3D printing of the denticle crown. This supporting material was carefully removed by water jet after the entire shark skin membrane was printed. The Objet Connex500 printer did not allow the denticles to be printed at-scale due to limitations on printing resolution: tests of at-scale 3D printing showed an unacceptable degradation of fine denticle structure. Therefore, we slightly exaggerated the denticle ridges while modeling to allow the printer to print denticles with sufficient surface topography. Thus, the denticle model in this paper (figure 1(b)) is slightly different from that used in our previous study (Wen *et al* 2014) and produced more biologically realistic final 3D surfaces from the printer. To accomplish this, we scaled the denticle ridges up gradually up from their original size until we obtained an acceptable size at which the ridges of the denticle were clearly identifiable in the final 3D prints. After a series of tests, synthetic denticles with clearly discernible 3D features such as the three surface ridges were obtained when the at-scale whole denticle model was magnified 12.4 times; denticle surface ridges were magnified 16.2 times their its original size to obtain a realistic surface pattern in the final print (figure 1(b)). More details of the 3D printing fabrication process are provided in our previous study (Wen *et al* 2014).

Wide-field scanning electron microscope (SEM) images of the 3D printed shark skin in a flattened state are provided in figures 2(a) and (b), and the 3D printed shark skin held in a curved state is shown in figure 2(c). The concave and convex wavy regions of the membrane demonstrate the flexibility of the whole sample. When the membrane substrate is curved, alterations in denticle overlap between the convex and concave regions can be easily observed, and the denticles contact and overlap anteriorly and posteriorly with each other in the concave region, and are spaced out in the convex area.

The smooth-surface control (figure 3(a)) and the three biomimetic shark skin membranes (figures 3(b)–(d)) were printed 55 mm in height and 165 mm in chord width, and the aspect ratio of the membranes was thus set as 0.33. Note that all four membranes were designed and printed at the same time with exactly the same mass (52.6 g). This was accomplished by slightly adjusting the thickness of the flexible black supporting material, and had no observable effect on the overall stiffness of the fully assembled membrane which is dominated by the stiffness of the central plastic support. Each printed membrane was glued onto a central plastic panel as in our previous work (Wen *et al* 2014). These central panels were made by laser-cutting plastic shim-stock material with a thickness of 0.508 mm, flexural stiffness of 9.8×10^{-4} N m^{-2}, and with a height the same dimension as the 3D printed membrane substrates (55 mm), and with a chord width 10 mm longer (175 mm) at the front. This design allowed the models to be clamped by a stainless steel sandwich bar (or spar) holder via small screws and held in the water tank during experiments. This attachment region is visible to the left of each membrane image in figure 3. The thickness of the stainless steel attachment spar equaled the thickness of two layers of 3D printed shark skin membrane plus the thickness of the central stiff supporting plastic element so that the leading edge of the moving membranes was formed by the stainless steel spar during the hydrodynamic tests in water tank, and the sides of the spar were level with the surface of the final assembled membranes. We refer to the completed biomimetic shark skin assembly as a membrane or panel.

2.2. Static and dynamic testing

A recirculating flow tank with a robotic flapping device mounted above it was used to investigate the hydrodynamics of the biomimetic shark skin and smooth control membranes for both static and dynamic (self-propelled) conditions as in our previous research (e.g., Lauder *et al* 2007, Oeffner and Lauder 2012, Quinn *et al* 2014). The flow tank had a rectangular cross-section of 25 cm by 30 cm with a 90 cm long working area and was filled with fresh water. The membranes were attached to a heave motor shaft with an ATI Nano-17 six-axis force/torque transducer (ATI Industrial Automation Inc., Apex, NC, USA) allowing for three forces (F_x, F_y, F_z) and three torques (T_x, T_y, T_z) to be measured simultaneously. Static drag force data consisted of nine data points for each membrane at speeds ranging from 0.1 m s^{-1} to 0.5 m s^{-1} with 0.05 m s^{-1} increments. The maximum tested speed of 0.5 m s^{-1} represents the maximum speed at which our flow tank could generate reasonable flows without excessive surface waves. The membranes were carefully aligned parallel to the direction of flow before each drag force measurement. Reported static drag

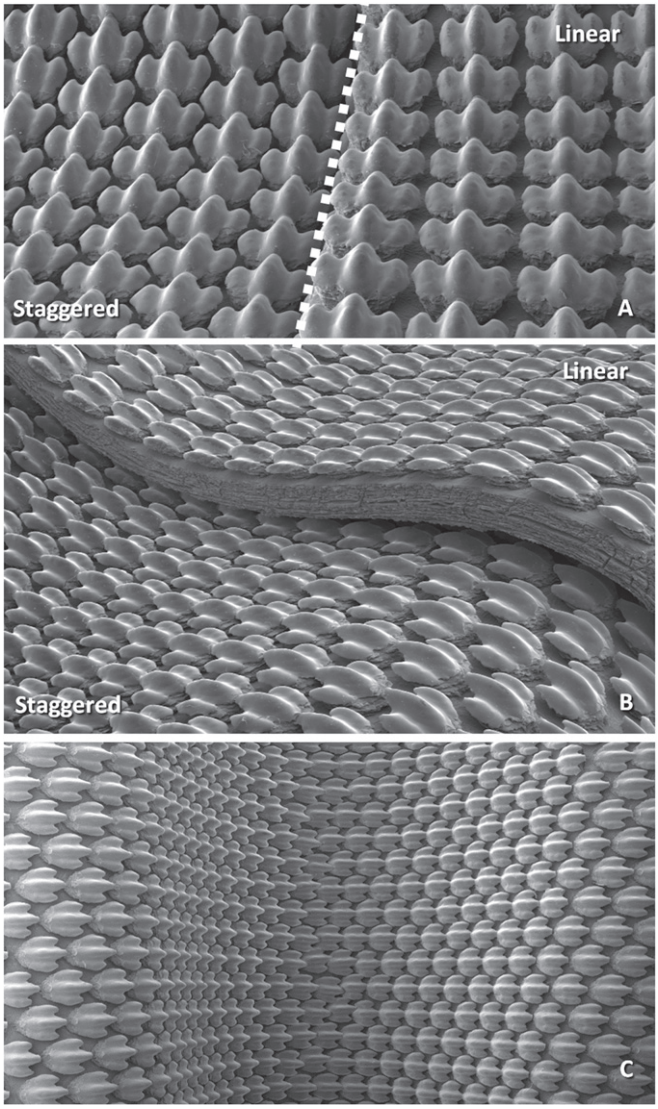

Figure 2. Scanning electronic microscope (SEM) images of the fabricated synthetic shark skin membranes. Staggered and linear arrays are shown from above (a) and from the side (b). These correspond to the patterns shown in figure 1 panels (d) and (e), respectively. Individual denticles are 1.1 mm in width. When the staggered-overlapped biomimetic shark skin membrane is curved (c), the denticles contact anteriorly and posteriorly with each other in the concave region, and spread out in the convex area.

force is the mean from five ($N = 5$) replicated trials for each measurement which lasted 10 s, sampled at 1000 Hz.

For the dynamic self-propelled swimming tests, the membranes were actuated with a heave (lateral, or side-to-side) motion at the leading edge following a sinusoid wave pattern as in previous work (e.g., Wen and Lauder 2013, Shelton *et al* 2014, Feilich and Lauder 2015). This induces curvature along the length of the membrane, and generates a traveling undulatory wave resulting in thrust production. In the current study, the amplitude (h) of the side-to-side heave motion was set to vary from ± 1 cm to ± 3 cm in 0.5 cm intervals, and all tests were conducted at a frequency (f) of 1 Hz. The self-propelled swimming speed (SPS) of each membrane was determined by finding the flow speed where the average thrust of the flapping panel average to zero using a custom LabVIEW program (Shelton *et al* 2014, Quinn *et al* 2014). We collected flapping panel force data using the mechanical flapping apparatus from our previous research (Alben *et al* 2012, Lauder *et al* 2012, Wen and Lauder 2013, Quinn *et al* 2014, Feilich and Lauder 2015). Force data was acquired for 10 s at 1000 Hz at nine different flow speeds near the expected self-propelled speed at intervals of 0.01 m s^{-1}. These force data were used to calculate the average thrust at each speed and a linear regression was fit to the nine data points to determine the self-propelled speed (when the mean thrust force is zero). Reported self-propelled speed is the mean from five ($N = 5$) replicated trials for each kinematic condition. The SPS speed for each membrane was then measured under each of the five different kinematic conditions. Image sequences of membrane midline kinematics were obtained using a Photron high-speed digital video cameras (Photron Inc., USA) with a

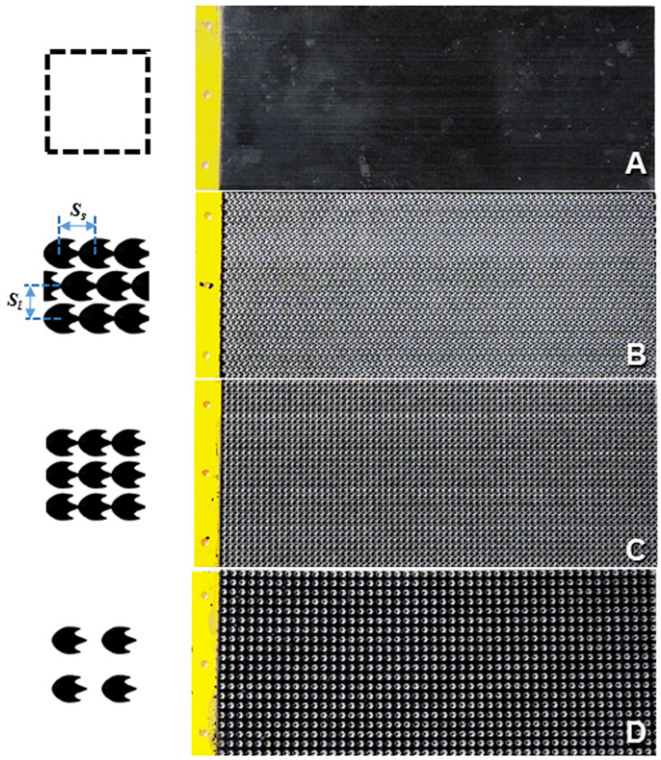

Figure 3. Flexible panels or membranes used to study the effect of denticle pattern and spacing on biomimetic shark skin propulsion. Denticle patterns are diagramed schematically to the left of each panel. A flexible plastic panel covered on both sides with a 3D printed smooth membrane is used as the control (a). The narrow exposed tab on the left allows attachment to the leading edge rod and mechanical controller. Staggered-overlapped (b), linearly-overlapped (c) and linearly-non-overlapped (d) arrayed biomimetic shark skin membranes were glued to a central plastic panel. S_s indicates the spacing between two adjacent denticles along the stream-wise direction. S_l indicates spacing between the mid-ridges of two adjacent denticles along the lateral direction. Detailed morphological parameters of shark skin membranes are provided in table 1. The smooth undersides of the synthetic shark skin membranes were glued to either side of a rectangular plastic element, so that the denticle-covered sides were exposed to the water flow during the experiments. Each shark skin membrane thus had shark skin denticles on two sides, while the control panel was smooth on both sides. Thickness of the flexible black supporting material was adjusted so that each assembled membrane had the same mass of 52.6 g.

resolution of 1024 pixels in both x and y dimensions. We digitized the flapping membranes for five replicate trials, and calculated the mean amplitude of the trailing edge of each flapping cycle. We calculated locomotor power as force times velocity of the heave motion (heave motion was tracked using an encoder on the heave motor). Power divided by the self-propelled swimming speed (SPS) gives the COT in J m^{-1} (also see Shelton *et al* 2014).

We focus in this paper on measuring self-propelled swimming speeds and testing under these conditions as we also have in several previous papers (Lauder *et al* 2012, Shelton *et al* 2014, Feilich and Lauder 2015 see Lauder *et al* 2007 for further discussion) because under self-propelled conditions thrust, side forces, and torques average zero over a flapping cycle. This provides a similar and natural testing condition to that of swimming in unrestrained live fishes which swim at self-propelled speeds and not under the influence of externally imposed forces. In addition, hydrodynamic flows over an undulating surface under non-self-propelled conditions are dramatically different than under self-propulsion (Lauder *et al* 2011), and to understand the effect of different denticle arrangements, it is important that the flexible biomimetic shark skin surfaces swim at their self-propelled speeds.

To compare the static drag force between the 3D printed shark skin and the smooth control membranes, we the used the ratio $D_{\text{shark}}/D_{\text{smooth}}$ (indicated as D_s/D_m in figure 4) as in Wen *et al* (2014). D_{shark} is the static drag of the shark skin membrane, and D_{smooth} is the static drag of the smooth control. This is termed the drag force ratio and indicates the relative drag force of the 3D printed shark skin and the smooth control. We also compared drag reduction performance of the 3D printed shark skin and smooth control membranes at a similar dimensionless parameter $S+$ based on previous studies of drag reduction by riblets (e.g. Anderson *et al* 1997, Bechert *et al* 1997), which showed that static drag reduction performance is dictated by the dimensionless parameter $S+$. $S+$ is an effective Reynolds number based on the spacing between riblets that reflects the gap between denticle top ridges:

$$S^+ = \frac{S}{\upsilon}\sqrt{\frac{\tau_w}{\rho}},$$

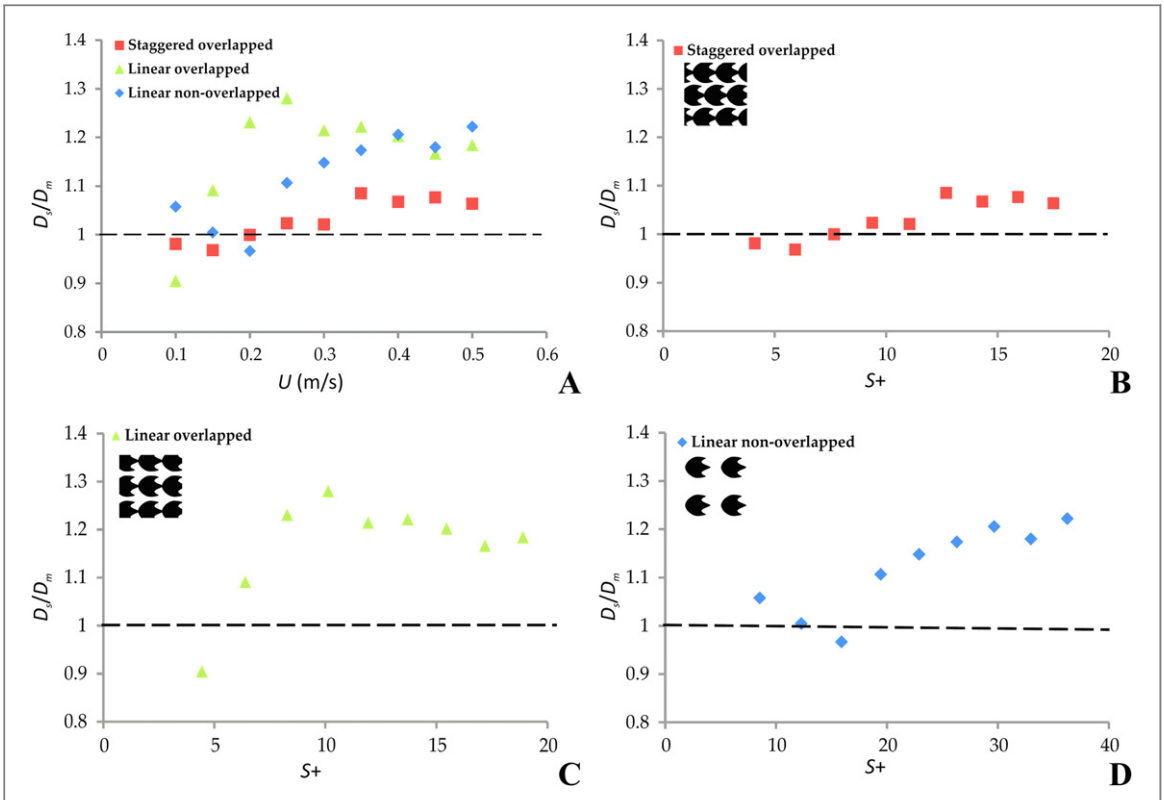

Figure 4. Static drag force ratio D_s/D_m dependence on the flow speed (a), and dimensionless denticle ridge spacing $S+$ of staggered-overlapped (b), linear-overlapped (c) and linear-non-overlapped (d) arrayed membrane. D_s represents the static drag of the shark skin membranes, and D_m represents the static drag of the smooth membrane. The dashed lines represent $D_s/D_m = 1$, which indicates that the synthetic shark skin membrane has the same static drag force as that of the smooth membrane. Separate plots are shown for each membrane pattern because the value of $S+$ differs slightly among membranes due to changes in denticle spacing. Drag forces of all membranes are means from five ($N = 5$) experimental trials for each experiment lasting 10 s.

where S is the spacing between adjacent denticle ridges, ρ is fluid density, ν is kinematic viscosity, and τ_w indicates the shear stress at the membrane surface (also see Wen *et al* 2014).

2.3. Statistical analysis

Differences among panels in self-propelled speed (SPS), power, and COT are reported as means of 5 trials (±one standard error). A two-way analysis of variance was used to test for differences among membrane types and heave amplitudes using JMP Pro 11.2.1 software (SAS Institute, Cary North Carolina) with both membrane type and heave amplitude as fixed effects. Tukey HSD post-hoc tests determined which biomimetic shark skin panels were significantly different from each other, and post-hoc least-square means contrast tests allowed comparison among groups of biomimetic panels.

3. Results

3.1. Static drag

Quantitative values of membrane Reynolds number (based on chord length) and static drag force data on all biomimetic and the smooth control panels are given in table 2. The ratios of drag forces on the shark skin membranes relative to the smooth control (D_s/D_m) and performance relative to the flow speed and dimensionless $S+$ are presented in figure 4. Static drag force for shark skin membranes generally increased as flow speed was increased from 0.1 m s^{-1} to 0.5 m s^{-1}. Increasing the flow speed and $S+$ resulted in an increasing drag ratio to a value of one (figure 4: dashed black line), which indicates that the biomimetic shark skin membranes and the control exhibited the same static drag force. All three biomimetic panels generate drag reduction at low flow speeds (figures 4(b)–(d)). At speeds above 0.20 m s^{-1} all shark skin membranes exhibited static drag values greater than the smooth control.

At a flow speed of 0.15 m s^{-1} ($U = 0.15$ m s^{-1}, $S+ = 6.4$), the staggered-overlapped shark skin showed drag reduction of 3.2%. Under the same flow speed U and $S+$, the static drag force of linear-overlapped panel increased 9%, while the linear-non-overlapped panel produced minimal drag reduction (0.4%). At the minimal tested flow speed ($U = 0.1$ m s^{-1}, $S+ = 4.43$), we found that the linear-overlapped membrane generated the maximum static drag reduction of 9.6% among all membranes.

Table 2. Dependence of static drag force on channel flow speed (U), and Reynolds number (Re_c). Static drag force data consists of 8 water tank flow speed points taken between 0.1 m s^{-1} and 0.5 m s^{-1} at increments of 0.05 m s^{-1}. Drag force measurements are the means of five ($N = 5$) replicate trials; error values are ±one standard error.

Water tank flow speed (U) (m s^{-1})	Chord Reynolds number (Re_c) $\times 10^3$	Control (mN)	Staggered-overlapped (mN)	Linear-overlapped (mN)	Linear-non-overlapped (mN)
0.1	16.5	2.5 ± 0.16	2.5 ± 0.18	2.3 ± 0.84	2.6 ± 0.32
0.15	24.7	4.6 ± 0.22	4.5 ± 0.21	5.1 ± 0.25	4.7 ± 0.63
0.2	33.0	8.6 ± 0.49	8.6 ± 0.44	10.6 ± 0.80	8.3 ± 0.50
0.25	41.2	13.2 ± 0.38	13.5 ± 1.63	16.9 ± 0.99	14.6 ± 0.37
0.3	49.5	20.5 ± 0.43	20.9 ± 1.16	24.8 ± 1.63	23.5 ± 0.42
0.35	57.7	28.2 ± 0.82	30.6 ± 1.32	34.5 ± 1.81	33.1 ± 0.54
0.4	65.9	37.7 ± 0.81	40.3 ± 1.58	45.4 ± 2.31	45.5 ± 0.71
0.45	74.2	47.8 ± 0.87	51.5 ± 2.37	55.7 ± 2.84	56.4 ± 0.46
0.5	82.4	59.6 ± 0.94	63.4 ± 1.66	70.6 ± 1.31	72.8 ± 0.74

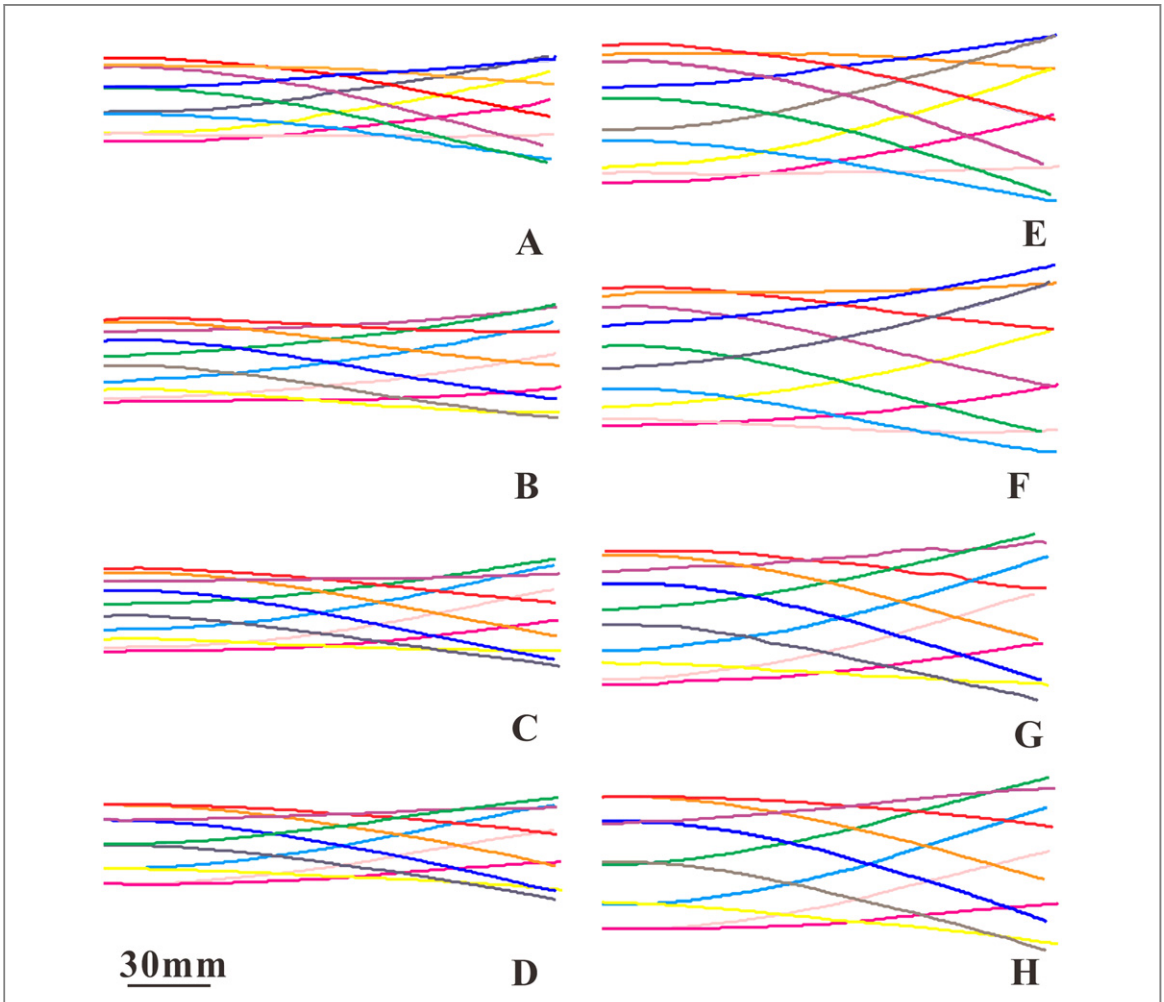

Figure 5. Midline snapshots of self-propelled membranes digitized from the ventral view. Midline kinematics of the control and three shark skin membranes at equally-spaced time intervals throughout a flapping cycle are illustrated. Midline kinematics were digitized from one representative trial as the motion was highly repeatable. Midline kinematics of all four membranes at motion of $f = 1$ Hz, $h = \pm 1.5$ cm are shown in (a), (b), (c) and (d) respectively. While midline kinematics of membranes at motion of $f = 1$ Hz, $h = \pm 2.5$ cm are shown in (e), (f), (g) and (h). The tip–tip amplitudes of trailing edges of flapping membranes are provided in table 3. From top to bottom in each column, membrane types are the smooth control, staggered-overlapped pattern, linear-overlapped pattern, and linear-non-overlapped pattern.

3.2. Membrane kinematics and self-propelled swimming speed

Biomimetic shark skin membrane midlines under self-propelled swimming conditions are shown at equally-spaced time intervals throughout an undulating cycle in figure 5, and tip-to-tip trailing edge amplitudes and Strouhal numbers are provided in table 3. We found that trailing edge amplitude varied with heave motion, denticle pattern, and spacing. The trailing edge amplitude of staggered-overlapped shark skin membranes is higher than that of linear-overlapped, linear-non-overlapped and smooth control

Table 3. Mean trailing edge tip-to-tip amplitude and Strouhal number values for the self-propelled swimming membranes at two different motions, $f = 1$ Hz, $h = \pm 1.5$ cm, and $f = 1$ Hz, $h = \pm 2.5$ cm.

e	Tip–tip amplitude (mm)		Strouhal number (St)	
Membrane	$f = 1$ Hz, $h = \pm 15$ mm	$f = 1$ Hz, $h = \pm 25$ mm	$f = 1$ Hz, $h = \pm 15$ mm	$f = 1$ Hz, $h = \pm 25$ mm
Control	39.1	62.5	0.2	0.2
Staggered-overlapped	42.3	68.4	0.2	0.2
Linear-overlapped	37.2	63.6	0.21	0.27
Linear-non-overlapped	41.2	63.1	0.26	0.28

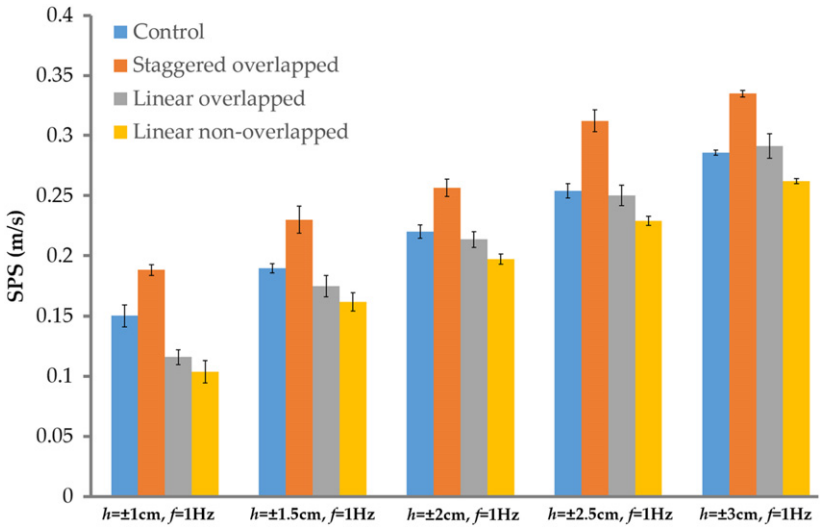

Figure 6. Histogram of the mean self-propelled swimming speed (SPS) of smooth control and synthetic shark skin panels as a function of heave amplitude at a fixed frequency of $f = 1$ Hz. Motion programs are indicated below the bars, which show the corresponding frequency (f) and amplitude (h). Error bars are ± 1 s.e.m. SPS values are averaged from five ($N = 5$) trials for each measurement.

membranes for all tested conditions. The staggered-overlapped panel produced larger trailing edge amplitudes than the other membranes at the two motion programs analyzed (table 3). For example, trailing edge tip-to-tip amplitude for the staggered-overlapped panel is 8.1% and 9.4% larger than for the smooth control under these two motion programs.

Self-propelled swimming (SPS) speeds for the five kinematic conditions are shown in figure 6 for heave values (h) of $h = \pm 1$ cm to ± 3 cm at 0.5 cm intervals. Self-propelled speed increases significantly with heave amplitude (ANOVA $P < 0.001$). All heave treatments produce generally similar effects among the different panel types, and the ANOVA membrane *heave interaction term was not significant ($P = 0.27$). ANOVA test of the membrane effect showed that the SPS speed also varied significantly with denticle pattern and spacing ($P < 0.001$), with the staggered-overlapped panel exhibiting the fastest swimming speed under all five conditions from $h = \pm 1$ cm to ± 3 cm. The staggered-overlapped shark skin membrane has a speed increase over the smooth control panel of 25.2% at 1 Hz $\pm$ 1 cm, 21.3% at ± 1.5 cm, 16.4% at ± 2 cm, 23.3% at ± 2.5 cm and 17.2% at ± 3 cm. The linear-overlapped and non-overlapped panel have lower self-propelled speeds than the smooth control for all swimming conditions, and the linear-non-overlapped panel shows the slowest swimming speeds under all motion programs (figure 6). For biomimetic shark skin membranes with the same denticle spacing, altering the denticle pattern from a linear to a staggered array significantly increased the SPS speed. Post-hoc Tukey HSD contrasts between the staggered-overlapped pattern and all other denticle conformations including the smooth control show that the staggered-overlapped membrane performs significantly better than any other membrane surface.

Strouhal numbers of the self-propelled swimming membranes are provided in table 3. The staggered-overlapped shark skin membrane produced the lowest Strouhal number (St = 0.20). In comparison, the linear-non-overlapped membrane generated highest Strouhal number (St = 0.28). The swimming panels all self-propelled at a Re range of 18 131–54 229 (table 2) and a St range of 0.2–0.28 (table 3).

3.3. Power consumption and COT

Swimming power was calculated for all biomimetic shark skin and the smooth control panels under five kinematic conditions (figure 7). Overall, power consumption of the biomimetic shark skin panels is higher than the smooth control, and the panel with the

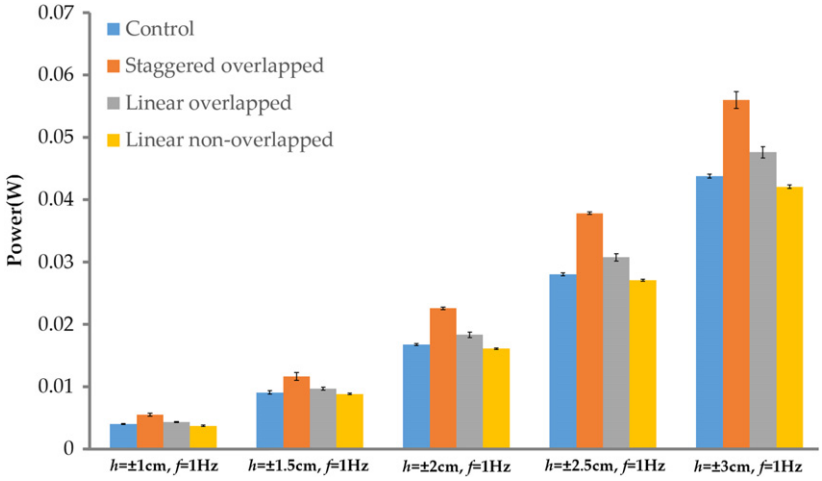

Figure 7. Histogram of the mean power consumption for smooth control and synthetic shark skin panels as a function of heave amplitude at fixed frequency $f = 1$ Hz. Motion programs are indicated below the bars, which show the corresponding frequency (f) and amplitude (h). Error bars are ± 1 s.e.m. Power values are averaged from five ($N = 5$) trials for each measurement.

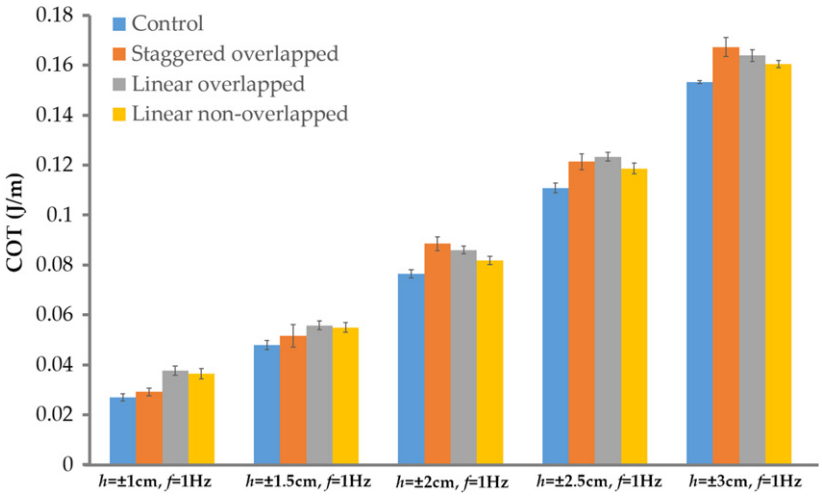

Figure 8. Histogram of the mean cost-of-transport (COT) for smooth control and synthetic shark skin membranes as a function of heave amplitude at frequency of 1 Hz. Motion programs are indicated below the bars, which show the corresponding frequency (f) and amplitude (h). Error bars are ± 1 s.e.m. COT values are averaged from five ($N = 5$) trials for each measurement.

staggered-overlapped denticle pattern consumed more power than other panels at all heave values. Compared with the smooth control panel, all biomimetic shark skin panels required more energy for swimming per unit distance (i.e. higher COT) (figure 8). Cost-of-transport for the staggered-overlapped membrane increased over the smooth control by 8.0% at ± 1 cm 1 Hz, 7.9% at ± 1.5 cm 1 Hz, 15.7% at ± 2 cm 1 Hz, 9.4% at ± 2.5 cm 1 Hz and 9.1% at ± 3 cm 1 Hz. However, the staggered-overlapped shark skin membrane generated much faster self-propelled swimming speed than other membranes, and as a result the increase in power consumption was counterbalanced by increased SPS speed, resulting in less of a relative increase in COT. Analysis of variance showed that the COT increased with heave amplitude (ANOVA $P < 0.001$), that there was a significant effect of membrane type ($P < 0.002$), but not a significant interaction term ($P = 0.11$). Post-hoc Tukey HSD contrasts showed that the COT for the staggered-overlapped pattern was not significantly different from the smooth control at the two lowest heave amplitudes. And, at the lowest heave value of ± 1 cm, the staggered-overlapped membrane pattern generated a lower COT than either the linear-overlapped and linear-non-overlapped membranes.

4. Discussion

4.1. A biomimetic approach to the dynamics of shark skin function

The ability to 3D print biomimetic shark skin with a flexible substrate and numerous rigid denticles which have an expanded base embedded into the flexible membrane (figures 1–3), allows testing of the

hydrodynamic effects of different denticle arrangements. As we have shown previously in dynamic tests using pieces of natural shark skin (Oeffner and Lauder 2012), flexibility of the shark skin surface is critically important to understanding the hydrodynamic performance of fish skin. The use of dynamic testing allows motion of the flexible skin surface of freely-swimming sharks to be replicated in a laboratory setting with a mechanical controller and recirculating flow tank, which provides for accurate measurement swimming forces, speeds, COT, kinematics, and hydrodynamics (Lauder and DiSanto 2015). Dynamic swimming tests of natural shark skin showed that the skin surface alters the vortex structure and flow in a manner that results in increased self-propelled swimming speeds (Oeffner and Lauder 2012). We thus regard the ability to reproduce flexibility of the skin surface and dynamic testing as necessary components of any attempt to understand shark skin function under swimming conditions. Even the surfaces of shark median and paried fins such as the pectoral fin undergo dynamic movements during swimming and maneuvering that result in flow separation and shed vorticity (Fish and Shannahan 2000, Wilga and Lauder 2000, 2001), and flow over the fin surface will be time-dependent and unsteady most of the time. Head oscillation during undulatory swimming also will enhance oscillatory flow over the pectoral fins. Recent computational work by Borazjani and Daghooghi (2013) has demonstrated a leading edge vortex on asymmetrical (heterocercal) tail structures similar to that seen on flexible shark skin membranes moved dynamically, and we suggest that the current body of experimental data from freely swimming sharks argues strongly for the value of using dynamic testing conditions with the associated ability to measure key experimental quantities associated with swimming performance.

The importance of testing under dynamic conditions is highlighted here by the contrast between our static drag data on the one hand, and self-propelled speed results on the other. Static drag tests show that at flow speeds above 0.2 m s^{-1}, all patterned biomimetic skin membranes experienced *increased* drag relative to the control (figure 4). This is likely to be due to the much greater surface area of each of the membranes with biomimetic shark skin denticles arrayed across the surface (table 1). The most densely packed biomimetic membrane is the staggered-overlapped design, and it has almost three times the total surface area of the smooth control (28 711 mm^2 compared to 10 420 mm^2), likely increasing static drag. However, when dynamic tests are conducted and speed is measured, the staggered-overlapped design swam significantly *faster* at all tested heave values (figure 6) than the smooth control. And at the two lower heave amplitudes, this occurred without any significant increase in the COT compared to the smooth control. Thus, static drag tests are not a reliable guide to the comparative swimming performance of flexible membranes, where flows over the surface are time-dependent, may involve separation around the leading edge (Oeffner and Lauder 2012), and bending of the surface changes the relationship of the patterned surface elements (Wen *et al* 2014; figure 2). Static tests could be relevant for a specific region where skin on live fishes does not oscillate during swimming, but we believe that such areas may be non-existent given the extent of body and head oscillation during shark locomotion and the more complex flows generated during lateral and vertical maneuvers which are a near-constant feature of the locomotor repertoire in sharks (Webb and Keyes 1982, Wilga and Lauder 2000, Shadwick 2005, Porter *et al* 2009, Lauder and DiSanto 2015).

Our previous research on natural shark skin function did not allow alteration of design parameters or investigation of how different arrangements of shark skin surface features might affect locomotor performance. The ability to 3D-print biomimetic shark skin with rigid denticles embedded into a flexible membrane now allows for realistic comparative testing under swimming conditions.

4.2. Effect of denticle pattern and spacing on locomotor performance

In this paper we present an analysis of three different denticle arrangements and the effect of changing arrangement and spacing on swimming performance. We chose to begin with three simple alterations of pattern while keeping the structure of individual denticles the same across all patterns. We altered the spacing and arrangement of surface denticles to better understand if spreading out denticles (and hence reducing total membrane surface area) might improve swimming performance, and altered the arrangement of denticles to compare performance of denticles in linear rows with a pattern in which denticle rows are offset to produce a staggered arrangement (figure 1). These patterns necessarily produced assembled flexible membranes with different numbers of denticles and total membrane surface areas (table 1). We expected *a priori* that the linearly-overlapped pattern (figure 1(e)) would exhibit the fastest self-propelled speed compared to the other patterns due to the alignment of denticles in distinct rows by analogy with surface riblet design (e.g., Anderson *et al* 1997, Bechert *et al* 1997). We also expected that the linearly-non-overlapped pattern might perform well during swimming due to its reduced total surface area compared with the other denticle patterns (figure 1(f)). Although the smooth control lacks denticles, it also has a much lower total surface area, and thus might show good swimming performance as well as low static drag. However, neither of these expectations was met, as the linearly-non-overlapped membrane exhibited the slowest self-propelled swimming speeds, and the

linearly-overlapped pattern was significantly slower than the staggered-overlapped pattern (figure 6).

In addition, a key feature of shark skin denticle design is the overlap between adjacent denticles in the upstream-downstream direction (Castro 2011, Motta *et al* 2012, Oeffner and Lauder 2012): the distal third of shark skin denticles in species like the bonnethead or mako sharks can overlap the next downstream denticle and denticles may interact physically during locomotion as the skin bends and flexes during undulatory propulsion. The two overlapped patterns were designed to examine this effect, and images of the manufactured 3D-printed biomimetic skin membranes clearly show denticle compression and overlap in valleys, and greater separation among denticles in the curved peak areas (figure 2).

Our results show that only one of the three biomimetic membrane patterns clearly outperformed both the smooth control and also the other two patterns during dynamic (swimming) tests: the staggered-overlapped pattern exhibited the highest self-propelled speeds at all tested heave conditions (figure 6). Even though the total surface area of the denticles plus membrane is almost three times that of the smooth control, swimming speeds were almost 20% faster on average. And the staggered-overlapped pattern performed considerably better than either the linear-overlapped pattern or the linear-nonoverlapped pattern. The smooth control swam faster than two of the three shark skin membranes at all heave amplitudes, but its performance never exceeded that of the staggered-overlapped pattern. Averaging the experimental trials of all heave motions, the staggered-overlapped shark skin membrane swam 20.1% faster than the smooth control, 26.4% faster than the linear-overlapped panel, and 38.5% faster than the linear-nonoverlapped panel. With regard to the COT, the staggered-overlapped panel on average cost 13.4% more than the smooth control when averaged over all heave amplitudes, but the COT was not significantly different than the smooth control at the two lowest heave amplitudes due to the substantially faster swimming speed which more than compensates for the increased power required (figure 8).

Differences in the COT between the staggered-overlapped pattern and the smooth control are not significant at the lowest heave values but increase as membrane curvature increases during faster swimming and higher heave values (figure 8). We suspect that this results from interactions among the denticles on the membrane surface: contact among denticles as the membrane bends back and forth (visible in the static images shown in figure 2) would increase energetic costs of swimming as the rigid denticles deform the flexible membrane at their base. For example, pressure from a downstream denticle on the undersurface of an upstream denticle in the concave region of a swimming membrane would force the upstream denticle to deform the flexible substrate through pressure at the expanded base. On our biomimetic shark skin membranes, physical contact and interaction among denticles would be expected to increase the COT.

However, in natural, fresh, shark skin, denticles are often very flexibly embedded into the dermis, and Motta *et al* (2012) and Lang *et al* (2011, 2014) have suggested that individual rigid denticles may alter their position in the skin passively to affect flow over the surface. We suggest that the mobility of denticles in sharks such as the pelagic mako (*Isurus oxyrinchus*) may also have another function: to reduce the energetic costs associated with bending the skin back and forth during undulatory locomotion. Possession of flexibly mounted dermal denticles could reduce costs incurred by physical denticle–denticle interactions, a design feature that we were not able to replicate in the biomimetic 3D-printed shark skin membranes studied here. Sharks with loosely-embedded denticles in the epidermis and dermis may be able to obtain the hydrodynamic advantages of denticle shape and patterning without incurring a higher COT due to contact among denticles and friction from denticles sliding past each other during skin bending.

4.3. Next steps in the study of biomimetic shark skin

Although for this first analysis of the effects of shark denticle patterning on locomotor performance we were able to 3D print rigid denticles on a flexible substrate in three different patterns, we did not vary the surface conformation of the denticles or explore a number of other potentially interesting avenues. One interesting direction for future work is study of the enormous variety of shark skin denticles and spacings present in different species. As denticle images in Castro (2011) show, skin denticles range in size from approximately 120 μm to more than 1000 μm, and show enormous diversity among species in the spacing among denticles and in shape. Denticles in some species are similar to pointed pyramids with sharp ends that extend more than a millimeter from the skin, while other species possess denticles shaped like paving stones and forming a flattened surface. Shark skin denticles also vary substantially in conformation around the body (Reif and Dinkelacker 1982, Reif 1985, Motta *et al* 2012), and species differ considerably in the spacing among denticles which can range from closely packed and overlapped to widely dispersed. The ability to 3D print denticles at smaller sizes in the future will enable testing at size scales closer to that of open ocean pelagic sharks that have relatively smaller denticles.

Understanding the effect of these different scale shapes and patterns requires an experimental approach in which individual parameters can be altered and controlled, and the effect of these alterations analyzed under dynamic swimming conditions. The ability to 3D-print different scale types and spacings will allow experimental manipulation of key

denticle parameters, and the ability to study near-skin hydrodynamic flow patterns during locomotion. Changing the mode of attachment of rigid denticles in the flexible membrane would also allow mobile denticles to be manufactured, and imaging of denticle–denticle interactions would permit exploration of the hypothesis that such interactions could increase the locomotor COT.

Acknowledgments

This work was supported by NSF grant EFRI-0938043 and ONR MURI Grant N000141410533 monitored by Dr Bob Brizzolara to GVL, China contract number 61403012 to Li Wen, and by the Wyss Institute for Biologically Inspired Engineering at Harvard University to JCW. Many thanks to Johannes Oeffner and Mark Ricco for their assistance imaging denticles with the ESEM and high-resolution micro-CT respectively. We thank members of the Lauder Lab for many helpful discussions on fish fins and flexible flapping membrane propulsion, and Erik Anderson, Vern Baker, Dan Quinn, and Chuck Witt for their considerable efforts in designing the robotic flapper and control software. Particular thanks is given to Ren Ziyu who helped design the SolidWorks model of the biomimetic shark skin, and assisted with data processing.

References

Alben S, Witt C, Baker T V, Anderson E J and Lauder G V 2012 Dynamics of freely swimming flexible foils *Phys. Fluids* A **24** 051901

Anderson E J, MacGillivray P S and Demont M E 1997 Scallop shells exhibit optimization of riblet dimensions for drag reduction *Biol. Bull.* **192** 341–4

Anderson E J, McGillis W and Grosenbaugh M A 2001 The boundary layer of swimming fish *J. Exp. Biol.* **204** 81–102

Applegate S 1967 A survey of shark hard parts *Sharks, Skates and Rays* ed W C Hamlett (Baltimore, MD: Johns Hopkins University Press) pp 37–67

Bechert D W, Bruse M, Hage W, Van Der Hoeven J G T and Hoppe G 1997 Experiments on drag-reducing surfaces and their optimization with an adjustable geometry *J. Fluid Mech.* **338** 59–87

Bhushan B 2011 Biomimetics inspired surfaces for drag reduction and oleophobicity/philicity *Beilstein J. Nanotechnology* **2** 66–84

Borazjani I and Daghooghi M 2013 The fish tail motion forms an attached leading edge vortex *Proc. R. Soc. London Biol. Sci.* **280** 20122071

Büttner C C and Schulz U 2011 Shark skin inspired riblet structures as aerodynamically optimized high temperature coatings for blades of aeroengines *Smart Mater. Struct.* **20** 094016

Castro J I 2011 *The Sharks of North America* (Oxford: Oxford University Press)

Dean B and Bhushan B 2010 Shark-skin surfaces for fluid-drag reduction in turbulent flow: a review *Phil. Trans. R. Soc.* A **368** 4775–806

Díez G, Soto M and Blanco J M 2015 Biological characterization of the skin of shortfin mako shark Isurus oxyrinchus and preliminary study of the hydrodynamic behaviour through computational fluid dynamics *J. Fish. Biol.* **87** 123–37

Feilich K L and Lauder G V 2015 Passive mechanical models of fish caudal fins: effects of shape and stiffness on self-propulsion *Bioinspir. Biomim.* **10** 036002

Fish F E and Shannahan L D 2000 The role of the pectoral fins in body trim of sharks *J. Fish. Biol.* **56** 1062–73

Kemp N E 1999 Integumentary system and teeth *Sharks, Skates, and Rays: The Biology of Elasmobranch Fishes* ed W C Hamlett (Baltimore, MD: Johns Hopkins University Press) pp 43–68

Lang A, Motta P, Habegger M L, Hueter R and Afroz F 2011 Shark skin separation control mechanisms *Mar. Tech. Soc. J.* **45** 208–15

Lang A W, Bradshaw M T, Smith J A, Wheelus J N, Motta P J, Habegger M L and Hueter R E 2014 Movable shark scales act as a passive dynamic micro-roughness to control flow separation *Bioinsp. Biomim.* **9** 036017

Lauder G V, Anderson E J, Tangorra J and Madden P G A 2007 Fish biorobotics: kinematics and hydrodynamics of self-propulsion *J. Exp. Biol.* **210** 2767–80

Lauder G V, Lim J, Shelton R, Witt C, Anderson E and Tangorra J L 2011 Robotic models for studying undulatory locomotion in fishes *Mar. Technol. Soc. J.* **45** 41–55

Lauder G V, Flammang B E and Alben S 2012 Passive robotic models of propulsion by the bodies and caudal fins of fish *Int. Comp. Biol.* **52** 576–87

Lauder G V and DiSanto V 2015 Swimming mechanics and energetics of elasmobranch fishes *Fish Physiology, Physiology of Elasmobranch Fishes: Structure and Interaction with Environment* vol 34A ed R E Shadwick *et al* (New York: Academic Press) pp 219–53

Meyer W and Seegers U 2012 Basics of skin structure and function in elasmobranchs: a review *J. Fish. Biol.* **80** 1940–67

Motta P, Habegger M L, Lang A, Hueter R and Davis J 2012 Scale morphology and flexibility in the shortfin mako *Isurus oxyrinchus* and the blacktip shark *Carcharhinus limbatus* *J. Morphol.* **273** 1096–110

Oeffner J and Lauder G V 2012 The hydrodynamic function of shark skin and two biomimetic applications *J. Exp. Biol.* **215** 785–95

Porter M E, Roque C M and Long J H 2009 Turning maneuvers in sharks: predicting body curvature from axial morphology *J. Morphol.* **270** 954–65

Quinn D B, Lauder G V and Smits A J 2014 Scaling the propulsive performance of heaving flexible panels *J. Fluid Mech.* **738** 250–67

Reif W and Dinkelacker A 1982 Hydrodynamics of the squamation in fast swimming sharks *Neues Jahrbuch Geol. Palaeontologie Abh.* **164** 184–7

Reif W-E 1985 Squamation and ecology of sharks *Cour. Forsch.-Inst. Senckenberg* **78** 1–255

Shadwick R 2005 How tunas and lamnid sharks swim: an evolutionary convergence *Am. Sci.* **93** 524–31

Shelton R M, Thornycroft P J M and Lauder G V 2014 Undulatory locomotion of flexible foils as biomimetic models for understanding fish propulsion *J. Exp. Biol.* **217** 2110–20

Webb P W and Keyes R S 1982 Swimming kinematics of sharks *Fish. Bull.* **80** 803–12

Wen L and Lauder G V 2013 Understanding undulatory locomotion in fishes using an inertia-compensated flapping foil robotic device *Bioinsp. Biomim.* **8** 046013

Wen L, Weaver J C and Lauder G V 2014 Biomimetic shark skin: design, fabrication and hydrodynamic function *J. Exp. Biol.* **217** 1656–66

Wilga C D and Lauder G V 2000 Three-dimensional kinematics and wake structure of the pectoral fins during locomotion in leopard sharks *Triakis semifasciata J. Exp. Biol.* **203** 2261–78

Wilga C D and Lauder G V 2001 Functional morphology of the pectoral fins in bamboo sharks, Chiloscyllium plagiosum: benthic versus pelagic station holding *J. Morphol.* **249** 195–209

Wilga C D and Lauder G V 2002 Function of the heterocercal tail in sharks: quantitative wake dynamics during steady horizontal swimming and vertical maneuvering *J. Exp. Biol.* **205** 2365–74

Zhao D-Y, Huang Z-P, Wang M-J, Wang T and Jin Y 2012 Vacuum casting replication of micro-riblets on shark skin for drag-reducing applications *J. Mater. Proc. Technol.* **212** 198–202